








RESEARCH ARTICLE | SEPTEMBER 20 2022

Conceptual study for velocity space resolved thermal ion loss detection in tokamaks

Special Collection: [Proceedings of the 24th Topical Conference on High-Temperature Plasma Diagnostics](#)

J. Poley-Sanjuán ; J. Galdón-Quiroga ; E. Viezzer ; J. Rueda-Rueda ; P. Cano-Megias ; P. Oyola ; D. J. Cruz-Zabala ; ASDEX Upgrade Team



Rev. Sci. Instrum. 93, 093511 (2022)

<https://doi.org/10.1063/5.0099087>



APL Energy

Latest Articles Online!

[Read Now](#)



Conceptual study for velocity space resolved thermal ion loss detection in tokamaks

Cite as: Rev. Sci. Instrum. 93, 093511 (2022); doi: 10.1063/5.0099087

Submitted: 14 May 2022 • Accepted: 28 July 2022 •

Published Online: 20 September 2022



View Online



Export Citation



CrossMark

J. Poley-Sanjuán,^{1,2,a)}  J. Galdón-Quiroga,¹  E. Viezzer,¹  J. Rueda-Rueda,¹  P. Cano-Megias,³ 
P. Oyola,¹  D. J. Cruz-Zabala,¹  and ASDEX Upgrade Team^{4,b)}

AFFILIATIONS

¹Department of Atomic, Molecular and Nuclear Physics, University of Seville, 41012 Seville, Spain

²Ecole Polytechnique Fédérale de Lausanne (EPFL), Swiss Plasma Center (SPC), CH-1015 Lausanne, Switzerland

³Department of Energy Engineering, University of Seville, 41012 Seville, Spain

⁴Max Planck Institute for Plasma Physics, 85748 Garching, Germany

Note: This paper is part of the Special Topic on Proceedings of the 24th Topical Conference on High-Temperature Plasma Diagnostics.

^{a)}Author to whom correspondence should be addressed: jesus.poley@epfl.ch

^{b)}See the author list of U. Stroth *et al.*, Nucl. Fusion **62**, 042006 (2022).

ABSTRACT

A new concept for velocity space thermal ion loss detection is presented. This diagnostic provides pitch angle resolved measurements that are unfeasible with current diagnostics. It uses the same detection principle as the Fast-Ion Loss Detector with a scintillator as the active component and includes a double slit configuration to measure simultaneously the escaping counter- and co-current ions. Simulations show a gyroradius range between 0.15 and 1.00 cm with a resolution below 0.15 cm (for a gyroradius of 1 cm) and a pitch angle range between 30° and 150° with a resolution below 8° for both counter- and co-current ions. The formation of a sheath in front of the detector and its associated electric field may impact the detection principle. Preliminary simulations with a homogeneous electric field show a decrease in the measurable velocity space range, whereas the gyroradius and pitch angle resolution barely change. The strike map is sensitive to the sheath electric field.

Published under an exclusive license by AIP Publishing. <https://doi.org/10.1063/5.0099087>

I. INTRODUCTION

The high confinement mode (H-mode) is one of the foreseen operational scenarios in future fusion devices due to its higher energy content and larger confinement time than the standard low confinement mode (L-mode).^{1,2} During the transition from L-to-H-mode, the so-called L–H transition, the radial electric field (E_r) plays an important role as the $\mathbf{E} \times \mathbf{B}$ shear is believed to decorrelate the fluctuations at the plasma edge, thus reducing the losses of energy and particles.^{2–4} This way, the confinement is improved leading to the H-mode pedestal formation. Thermal ion losses may contribute partially to the formation of E_r and, therefore, to the L–H transition.^{5–8} Therefore, characterizing the thermal ion loss velocity space contributes to a deeper understanding of the thermal ion loss cone and potentially to the L–H transition. This characterization is not provided by current diagnostics such as the retarding field analyzer. Therefore, a conceptual study for a new diagnostic, the Thermal Ion Loss Detector (TILD), is presented in this paper.

This paper is structured as follows: the TILD working principle is explained in Sec. II. In Sec. III, the optimal position and the design of the diagnostic are explained including the resolution of the detector, while Sec. IV introduces the response of TILD to the misalignment between the magnetic field and the detector head and to the sheath formation.

II. WORKING PRINCIPLE

The proposed diagnostic principle is based on the widely used scintillator based Fast-Ion Loss Detector (FIELD).⁹ It is based on the motion of a charged particle along the magnetic field. As shown in Fig. 1, in the poloidal projection of the ASDEX Upgrade (AUG) vacuum vessel, a lost ion following the magnetic field line [in red extending outside the plasma in the Scrape-Off layer (SOL)] will intercept a hole in the detector head, the so-called pinhole. Among all the ions that enter the pinhole, only a fraction of them will go

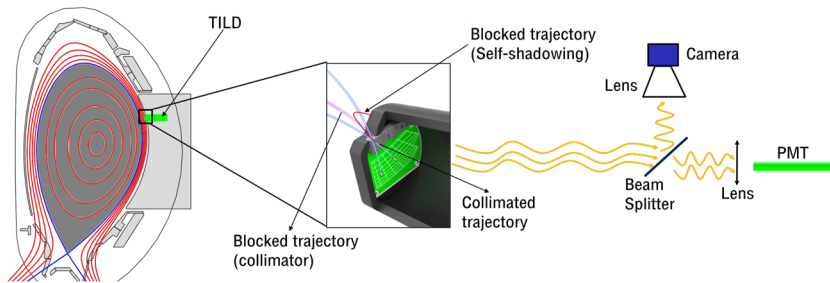


FIG. 1. TILD working principle: a lost ion enters the collimator and, if not blocked, it produces light acquired by a camera and a PMT. Reproduced with permission from J. Galdon-Quiroga *et al.*, Plasma Phys. Controlled Fusion **60**, 105005 (2018). Copyright 2018 IOPSCIENCE.

all the way through the collimator to hit the active component plate. This fraction is the so-called collimator factor, f_{col} . The ions will collide in different positions of the plate depending on their velocity and, hence, their gyroradius and pitch ($\xi = -v_{\parallel}/v$, where \parallel is the direction of the magnetic field). If the active component is a scintillator, as in other similar diagnostics such as FILD⁹ and Imaging Neutral Particle Analyzer^{10,11} (INPA), then light is emitted when the ion hits the plate. As depicted in Fig. 1, the light goes to a beam splitter where it is divided into a high spatial resolution system (lens plus camera) and a high temporal resolution system [usually an array of optical fibers connected to a Photo Multiplier Tube (PMT)]. This way, the camera allows the resolved measurement in pitch angle and gyroradius, while the fast acquisition provides information about the interaction of the ions with instabilities and complementary information of the camera measurements. Some ions will collide with the head of the detector before entering through the pinhole, which is the so-called self-shadowing effect.

III. POSITIONING AND DESIGN OF TILD

To do a first estimation of the most suitable poloidal location of TILD, the threshold energy that the ion needs to have to be able to cross the separatrix has been estimated for the different AUG

poloidal regions. This calculation is based on the energy, canonical toroidal angular momentum ($p_{\phi} = rmv_{\parallel}f_{\phi} + e\psi$, where r is the radial position, m is the mass, $f_{\phi} = |B_{\phi}/B|$, e is the electron charge, and ψ is the poloidal magnetic flux), and the magnetic moment (μ) conservation assuming a collisionless trajectory.^{8,12,14} As shown in Fig. 2, the minimum threshold energy to cross the separatrix for both co- and counter-current ions is around the outer midplane (black) for deeply passing ions. This is in accordance with the results presented in Ref. 12. Therefore, as a first estimation, it seems that the outer midplane region would be most appropriate to locate TILD.

The detector has been designed taking into account three factors: the energy range of the thermal ions and the self-shadowing effect, the collimator factor, and the energy and pitch resolution. To do the optimization and design of the geometry, the FILDSIM¹³ code has been used.

A. Self-shadowing

Due to the energy range of the thermal ions (≤ 1.5 keV, gyroradius ≤ 0.7 cm, for a local magnetic field of $B = 1.5$ T, and calculated with the total velocity), the self-shadowing effect may play an important role since a large part of the ions could be blocked by the geometry itself. To avoid this, the pinholes are located as close to the side of the head as possible, as shown in Fig. 3.

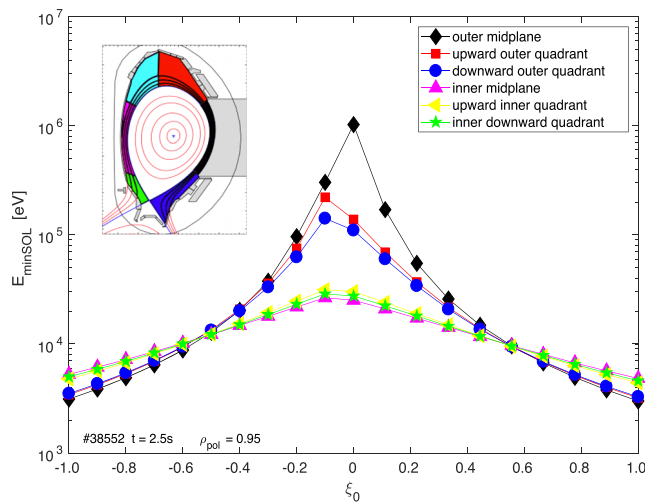


FIG. 2. Minimum threshold energy for the thermal ions to cross the separatrix and be lost depending on the poloidal region vs the initial pitch (ξ_0).

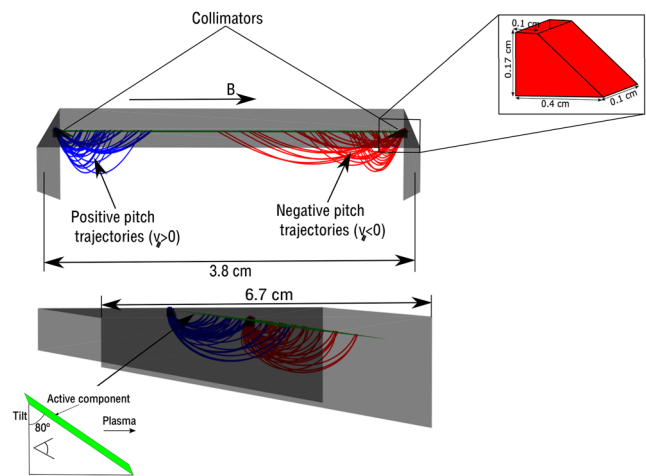


FIG. 3. TILD geometry including its dimensions, the collimator dimensions, and the tilt of the active component.

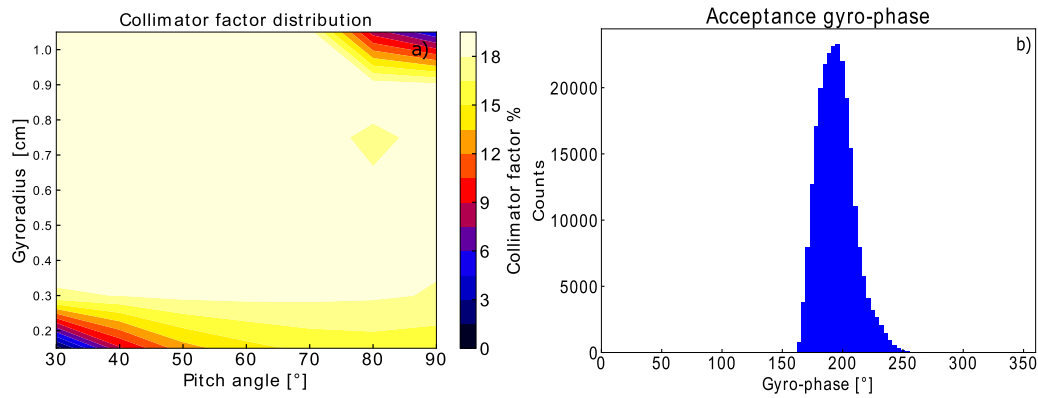


FIG. 4. Collimator factor contour for the gyroradius and pitch angle pairs (a) and gyro-phase acceptance range (b).

B. Collimator factor

The collimator factor ($f_{col} = N_{hit}/N_{pinhole}$) provides information of how many of the ions entering the pinhole ($N_{pinhole}$) finally hit the active component (N_{hit}). If the pinhole is smaller, the resolution of the detector, in other words, the spreading in energy and pitch would be smaller too, as well as the measured signal decreases. Hence, it is a trade-off between the resolution and the measured signal. In this case, to collimate the ion distribution at the pinhole means to reduce the ion gyro-phase distribution. As shown in Fig. 4(a), for the design of the collimator shown in Fig. 3, the collimator factor is below 20%, and as shown in Fig. 4(b), the gyro-phase acceptance range is around 70°. It can be seen that f_{col} decreases with the gyroradius, as expected, and the pitch angle due to the geometry of the collimator. Based on the typical values of FILD detectors ($f_{col} \sim 4\%$ ¹³), it seems that the collimation could be higher, i.e., the distributions could be further collimated. The design of TILD also includes two collimators, one on each side, to measure both co- and counter-current ions, obtaining this way a larger adaptability to different plasma scenarios.¹⁵ The design of the collimator and pinhole is the same for both. This leads to an acceptance gyroradius range

between 0.15 and 1 cm, and a pitch angle [$\Lambda = \arccos(\xi)$] range between 20° and 150°.

C. Energy and pitch resolution

Apart from the collimation, the position of the active component plays an important role in the spread of the ions and, hence, in the resolution of the detector. Since the range of gyroradius intended to be measured goes from 0.15 to 1 cm, the active component has to be placed very close to the collimator to catch the lower energy ions, but at the same time, it has to be placed further away from the collimator to increment the separation between the distributions of higher energy ions. Therefore, to satisfy both conditions simultaneously, the active component is tilted with respect to the vertical plane instead of being parallel to it as in FILD detectors. As shown in Fig. 5, this leads to a “banana” shape distribution of the strike points in the active component plate.

Using this geometry, the resolution of the detector can be computed, i.e., the deviation from the centroid of the distributions for each gyroradius and pitch angle pair. This is shown in the contours of Fig. 6, where the sigma values come from the sigma of the

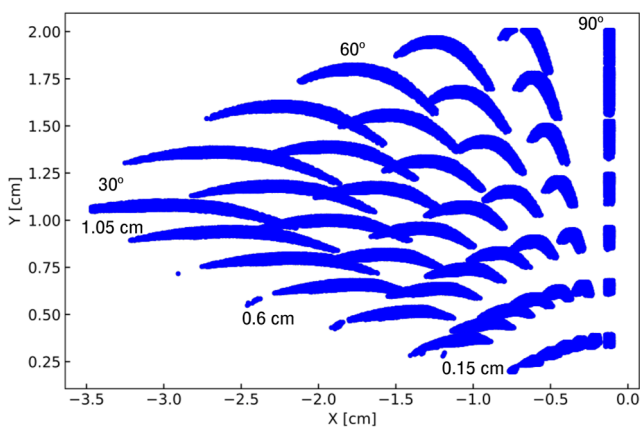


FIG. 5. Strike points distributions on the tilted active component.

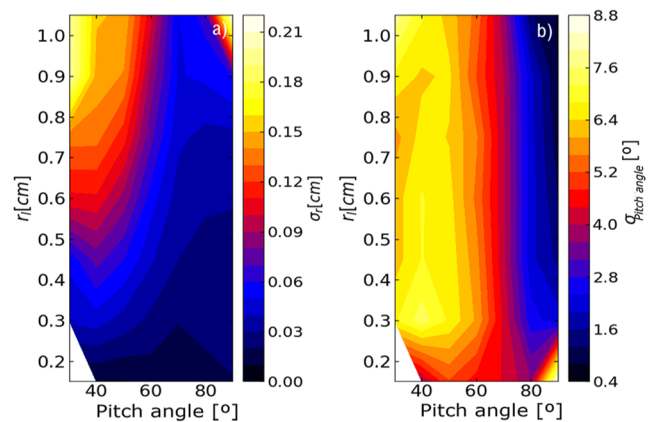


FIG. 6. Resolution contours in gyroradius (a) and pitch angle (b) for each velocity space pair.

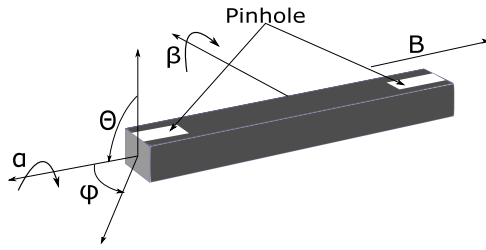


FIG. 7. Angle criteria to describe the alignment between the magnetic field and the detector. The rotation of the head of the detector is described by the angle β .

Gaussian distribution fitted to the strike points. It can be noted that the resolution in gyroradius gets worse for larger values and smaller pitch angles. This is in accordance with the collimator factor contour (Fig. 4) and the strike point distributions (Fig. 5)—the collimation is smaller for larger gyroradius and smaller pitch angle, which leads to a wider spread in the gyro-phase of the strike points. In the case of the pitch resolution, it is almost constant for the gyroradius values, but it gets worse for smaller pitch angles, which is also in accordance with the strike points plot (Fig. 5).

IV. SENSITIVITY TO RADIAL INSERTIONS AND THE SHEATH FORMATION

The misalignment between the local magnetic field and the pinhole plane could impact the amount of signal for small gyroradius and pitch angle cases due to the larger amount of ion trajectories blocked by the collimator. The misalignment varies with the local magnetic field and, therefore, it could play an important role if fast radial insertions are used or if the magnetic equilibrium changes considerably. As shown in Fig. 7, in order to describe the alignment, two angles are introduced—the angle from the horizontal plane toward the vertical direction, Θ , and the angle between the radial direction and the projection of the magnetic field (B) in the horizontal plane, ϕ . If those angles are 0° , then the detector and the magnetic field are perfectly aligned. To achieve the alignment, two angles can be modified: the rotation of the head, β , and the angle of the head of the detector with respect to the radial direction, α

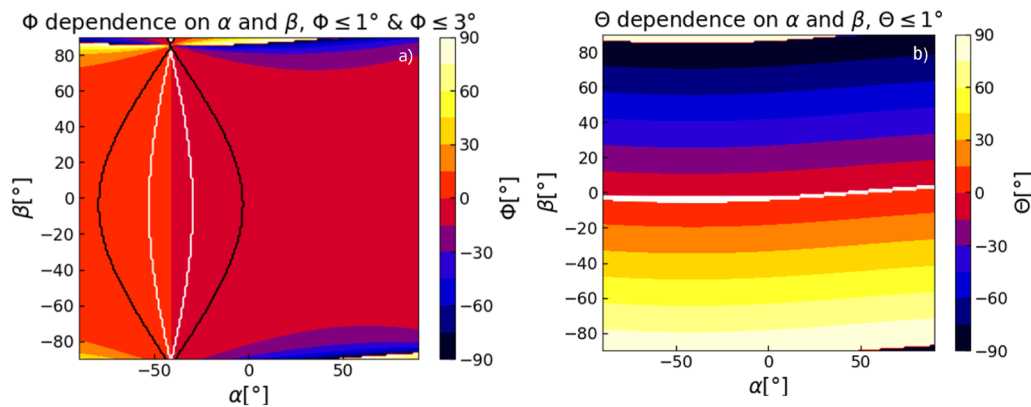


FIG. 8. Dependence of the angles ϕ and Θ with the rotation of the head around the radial direction, β , and around the vertical direction, α . In (a), the black line indicates where $\phi \leq 3^\circ$, and the white line indicates where $\phi \leq 1^\circ$. In (b), the white area indicates where $\Theta \leq 1^\circ$.

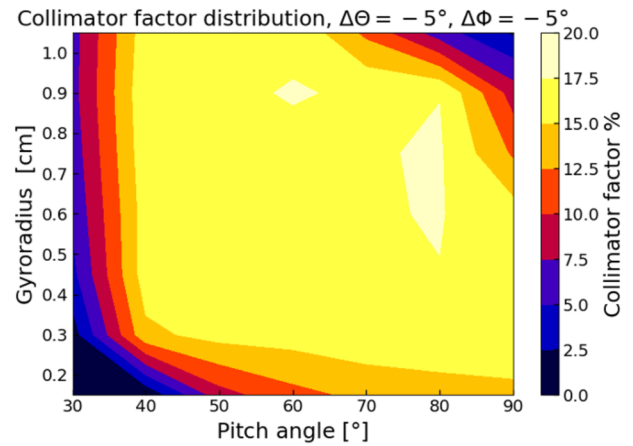


FIG. 9. Collimator factor for the gyroradius and pitch angle pairs with a misalignment of $\Delta\Theta = 5^\circ$ and $\Delta\phi = 5^\circ$.

(Fig. 7). The dependence of ϕ and Θ , i.e., the alignment, with α and β is shown in Fig. 8. As shown, to reduce the misalignment, i.e., ϕ and Θ close to 0° , there is a strong dependence on the β values, whereas there is no such dependence on the α values. Hence, to prevent misalignment by rotation of the head of the detector along the β angle is proposed.¹⁶

The impact on the alignment of the detector head with respect to the magnetic field has been addressed. A radial insertion in the outer midplane of up to 1 cm leads to a maximum misalignment in both Θ and ϕ of $\sim 5^\circ$. As shown in the collimator factor contour in Fig. 9, the misalignment leads to a decrease in the number of ions hitting the active component mainly for the small pitch angle cases ($\lambda < 40^\circ$). However, only for gyroradius smaller than 0.3 cm, this seems to be critical.

Since the detector is inserted in the SOL region, an accumulation of negative charge in the head of the detector is expected, i.e., a sheath layer.¹⁷ The accumulation of charge can lead to a voltage drop of $V_{sheath} \sim -20$ V in a characteristic length of $L_{sheath} \sim 35\lambda_D \sim 10^{-3}$

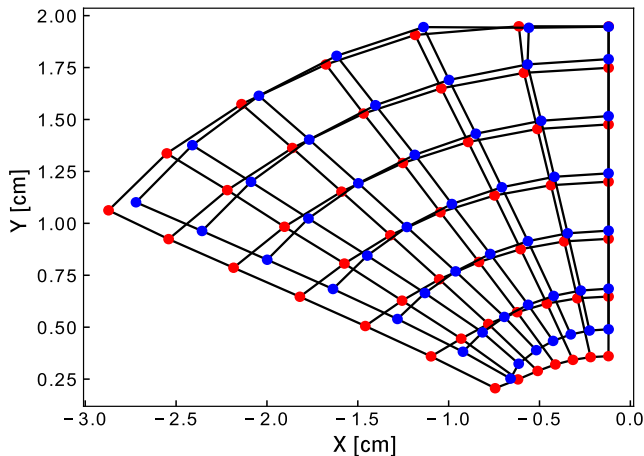


FIG. 10. Strike map without (red) and with (blue) the 20 kV/m electric field.

m, where λ_D is the Debye length (λ_D), which considering an electron density of $n_e \sim 10^{19} \text{ m}^{-3}$ and a temperature (T) of $T \sim 20 \text{ eV}$, is of the order of 10^{-5} m . As a first estimate, the effect of the sheath electric field has been simulated assuming a homogeneous 20 kV/m field using the upgraded FILDSIM code.¹⁸ As shown in Fig. 10, the strike map (made by linking the centroids of the distributions of striking ions) when applying the homogeneous 20 kV/m electric field changes with respect to the baseline case without field. Therefore, this effect has to be considered when interpreting the position of the strikes in the active component plate. A possible solution to have larger certainty about V_{sheath} would be to bias negatively the head with a well-known voltage avoiding the accumulation of extra negative charges. This way, the sheath effect could be addressed for interpreting the measurements.

V. CONCLUSIONS

The conceptual study of a new detector able to measure the velocity space of thermal ion losses with high spatial and temporal resolution is presented. The diagnostic is based on the same working principle of a FILD detector with a double collimator and a rotary head design to provide more adaptability to different magnetic and plasma scenarios. TILD would have a size of $6.7 \times 3.8 \text{ cm}^2$ with the spots being typically of $0.5 \times 0.3 \text{ cm}^2$. By using the design presented, the detector shows a resolution in gyroradius below 0.21 cm ($<0.3 \text{ keV}$, for a local $B = 1.5 \text{ T}$) and in pitch angle below 8° . The sheath layer that forms in the head of the detector has to be taken into account when interpreting the data. The detector could be biased to infer the effect of the sheath on the measurements. As it has been seen, the strike map will change accordingly, whereas the velocity space range will not be reduced. Further work is needed to address the impact of the sheath electric field, to determine the most appropriate active component, and to address the compatibility of the probe head design with the expected heat loads close to the separatrix.

ACKNOWLEDGMENTS

This project has been developed in the framework of the 2020 Leonardo Grants for Researchers and Cultural Creators of

the BBVA Foundation. The BBVA Foundation is not liable for the opinions, comments, and contents included in the project and/or the results derived from it, being the sole and exclusive responsibility of its authors. E.V. gratefully acknowledges the support from the European Research Council (ERC) under the European Union's Horizon 2020 research and innovation program (Grant Agreement No. 805162). J.G.-Q. acknowledges the support from the Spanish Ministry of Science and Innovation under Grant No. FJC2019-041092-I.

AUTHOR DECLARATIONS

Conflict of Interest

The authors have no conflicts to disclose.

Author Contributions

Jesus Poley Sanjuán: Conceptualization (lead); Formal analysis (lead); Investigation (lead); Writing – original draft (lead); Writing – review & editing (lead). **Joaquín Galdon-Quiroga:** Methodology (equal); Project administration (equal); Resources (supporting); Supervision (equal); Writing – review & editing (equal). **Eleonora Viezzer:** Methodology (equal); Project administration (equal); Resources (supporting); Supervision (equal); Writing – review & editing (equal). **Jose Rueda-Rueda:** Resources (supporting); Software (supporting); Writing – review & editing (equal). **Pilar Cano-Megias:** Resources (supporting); Writing – review & editing (equal). **Pablo Oyola:** Resources (supporting); Software (supporting); Writing – review & editing (supporting). **Diego Jose Cruz-Zabala:** Resources (supporting); Writing – review & editing (supporting).

DATA AVAILABILITY

The data that support the findings of this study are available from the corresponding author upon reasonable request.

REFERENCES

- 1 F. Wagner *et al.*, *Phys. Rev. Lett.* **49**, 1408 (1982).
- 2 E. Wolfrum *et al.*, in 25th IAEA International Conference on Fusion Energy, 2014.
- 3 H. Biglari, P. H. Diamond, and P. W. Terry, *Phys. Fluids B* **2**, 1–4 (1990).
- 4 F. L. Hinton, *Phys. Fluids B* **3**, 696–704 (1991).
- 5 K. C. Shaing and E. C. Crume, Jr., *Phys. Rev. Lett.* **63**, 2369 (1989).
- 6 C. S. Chang, S. Kue, and H. Weitzner, *Phys. Plasmas* **9**, 3884–3892 (2002).
- 7 Q. An *et al.*, *Phys. Rev. Lett.* **118**, 089602 (2017).
- 8 R. W. Brzozowski III *et al.*, *Phys. Plasmas* **26**, 042511 (2019).
- 9 M. Garcia-Munoz *et al.*, *Rev. Sci. Instrum.* **80**, 053503 (2009).
- 10 J. Rueda-Rueda *et al.*, *Rev. Sci. Instrum.* **92**, 043554 (2021).
- 11 X. D. Du *et al.*, *Nucl. Fusion* **58**, 082006 (2018).
- 12 W. M. Stacey, *Nucl. Fusion* **53**, 063011 (2013).
- 13 J. Galdon-Quiroga *et al.*, *Plasma Phys. Controlled Fusion* **60**, 105005 (2018).
- 14 T. M. Wilks and W. M. Stacey, *Phys. Plasmas* **23**, 122505 (2016).
- 15 L. Stipani, Ph.D. thesis, EPFL, 2021.
- 16 J. F. Rivero-Rodríguez *et al.*, *Rev. Sci. Instrum.* **89**, 10I112 (2018).
- 17 I. H. Hutchinson, *Principles of Plasma Diagnostics* (Cambridge University Press, 2002), ISBN: 9780511613630.
- 18 J. Rueda-Rueda *et al.* “Commissioning of the Imaging Neutral Particle Analyser at the ASDEX Upgrade tokamak” (unpublished).